ARCHIVES OF ELECTRICAL ENGINEERING VOL. 64(1), pp. 89-105 (2015)

DOI 10.1515/aee-2015-0009

Modelling and performance analysis of dual-channel switched reluctance motor

PIOTR BOGUSZ, MARIUSZ KORKOSZ, JAN PROKOP

Rzeszow University of Technology
Faculty of Electrical and Computer Engineering
ul. Wincentego Pola 2, 35-959 Rzeszów, Poland
e-mail: pbogu/mkosz/jprokop@prz.edu.pl

(Received: 28.10.2014, revised: 22.12.2014)

Abstract: The paper is a presentation of an analysis concerning performance of a 12/8 dual-channel switched reluctance motor (DCSRM). Formulas constituting a base for a non-linear mathematical model of DCSRM are presented. Simulation and laboratory tests were carried out for the motor operating in the dual-channel and single-channel mode. The results of the field theory-based calculations are presented in the form of fluxes in individual phases expressed as functions of currents and a rotor position angle. The results of the computer simulations are shown as the static characteristics of fluxes and the torque as well as voltage, current, and torque waveforms. The results of the laboratory tests are also presented.

Key words: dual channel switched reluctance motor, DCSRM, mathematical model, SRM

1. Introduction

The so-called critical drives, e.g. fuel pump drives in aircraft or electric motorcar propulsion systems, are nowadays expected to be highly resistant to failures of both the electric motor and the motor supplying circuit. A solution potentially capable to meet requirements imposed on critical drives consists in selection of the dual-channel switched reluctance motor (DCSRM) [1-5]. DCSRMs can be used in the so-called dual-channel operation mode, where corresponding phases of both channels are supplied at the same time, or in the single-channel operation mode [1-3]. In a failure condition consisting in damage of a phase winding in one of the channels or a malfunction of the circuit supplying the channel, the motor is capable to operate in the single-channel mode, allowing thus to maintain the drive operation continuity.

The purpose of the present paper is to present an analysis of performance of a DCSRM carried out on the grounds of simulation and laboratory tests performed on a three-phase dual-channel DCSRM.

Figure 1 shows the cross-section of a 12/8 DCSRM with one phase of channel A (u_1^A, i_1^A) and channel B (u_1^B, i_1^B) marked as an example.

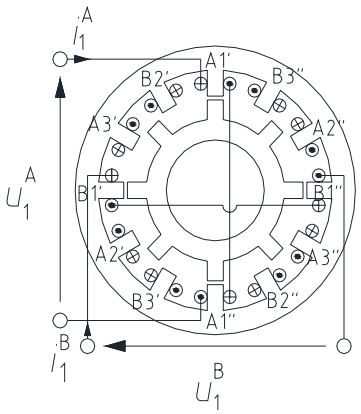

Fig. 1. A schematic view of cross-section of a 12/8 three-phase DCSRM

Figure 2 presents a schematic diagram of the circuit supplying a three-phase DCSRM with converter circuits supplying channel A and channel B windings. The examined motor can be operated in the so-called dual-channel mode where the corresponding phases of both channels A and B are pulse-like supplied at the same time or in the single-channel operation mode where the pulsed supply is provided only to phases of one of the channels, A or B.

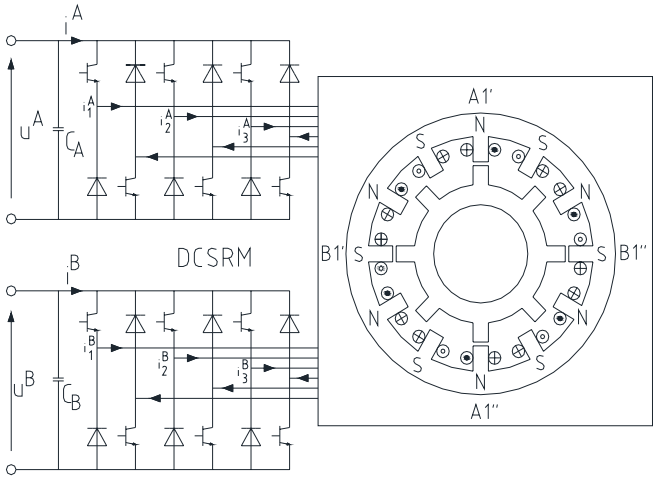

Fig. 2. A schematic diagram of the circuit supplying a 12/8 three-phase DCSRM

For the examined DCSRM, a mathematical circuit model has been developed taking into account non-linearity of the magnetic circuit and mutual linkages both between windings of a given channel (A or B) and between phases of two different channels (A and B). The paper presents results of simulations that were further verified by means of laboratory measurements.

2. A mathematical model of DCSRM

To model a three-phase DCSRM, the so-called flux-based field-circuit model with indirect linkage has been used. In such a model, the functional dependence of relevant fluxes on the rotor position and phase currents were determined by means of 2D field methods, and then the set of the obtained relationships was used in the circuit model. The machine model discussed here takes into account the non-linearity of the magnetisation characteristics and all linkages existing between phases of both channels. For the purpose of the present model it is assumed that the fluxes of the individual phases for both channels, A and B, can be expressed as the sums of the fluxes depending on the rotor position angle and only one phase current in a given channel, according to the definition [6, 9]

$$\boldsymbol{\psi}^{\mathrm{A}}(\theta,\mathbf{i}^{\mathrm{A}},\mathbf{i}^{\mathrm{B}}) = \boldsymbol{\psi}^{\mathrm{AA}}(\theta,\mathbf{i}^{\mathrm{A}}) + \boldsymbol{\psi}^{\mathrm{AB}}(\theta,\mathbf{i}^{\mathrm{B}}), \tag{1}$$

$$\boldsymbol{\psi}^{\mathrm{B}}(\theta,\mathbf{i}^{\mathrm{A}},\mathbf{i}^{\mathrm{B}}) = \boldsymbol{\psi}^{\mathrm{BA}}(\theta,\mathbf{i}^{\mathrm{A}}) + \boldsymbol{\psi}^{\mathrm{BB}}(\theta,\mathbf{i}^{\mathrm{B}}), \tag{2}$$

where:

$$\boldsymbol{\psi}^{\mathrm{AA}}(\theta,\mathbf{i}^{\mathrm{A}}) = \begin{bmatrix} \sum_{j=1}^{3}\psi_{1j}^{\mathrm{AA}}(\theta,i_j^{\mathrm{A}}) \\ \sum_{j=1}^{3}\psi_{2j}^{\mathrm{AA}}(\theta,i_j^{\mathrm{A}}) \\ \sum_{j=1}^{3}\psi_{3j}^{\mathrm{AA}}(\theta,i_j^{\mathrm{A}}) \end{bmatrix}, \qquad \boldsymbol{\psi}^{\mathrm{AB}}(\theta,\mathbf{i}^{\mathrm{B}}) = \begin{bmatrix} \sum_{j=1}^{3}\psi_{1j}^{\mathrm{AB}}(\theta,i_j^{\mathrm{B}}) \\ \sum_{j=1}^{3}\psi_{2j}^{\mathrm{AB}}(\theta,i_j^{\mathrm{B}}) \\ \sum_{j=1}^{3}\psi_{3j}^{\mathrm{AB}}(\theta,i_j^{\mathrm{B}}) \end{bmatrix}, \tag{3}$$

$$\boldsymbol{\psi}^{\mathrm{BA}}(\theta,\mathbf{i}^{A}) = \begin{bmatrix} \sum_{j=1}^{3}\psi_{1j}^{\mathrm{BA}}(\theta,i_j^{\mathrm{A}}) \\ \sum_{j=1}^{3}\psi_{2j}^{\mathrm{BA}}(\theta,i_j^{\mathrm{A}}) \\ \sum_{j=1}^{3}\psi_{3j}^{\mathrm{BA}}(\theta,i_j^{\mathrm{A}}) \end{bmatrix}, \qquad \boldsymbol{\psi}^{\mathrm{BB}}(\theta,\mathbf{i}^{B}) = \begin{bmatrix} \sum_{j=1}^{3}\psi_{1j}^{\mathrm{BB}}(\theta,i_j^{\mathrm{B}}) \\ \sum_{j=1}^{3}\psi_{2j}^{\mathrm{BB}}(\theta,i_j^{\mathrm{B}}) \\ \sum_{j=1}^{3}\psi_{3j}^{\mathrm{BB}}(\theta,i_j^{\mathrm{B}}) \end{bmatrix} \tag{4}$$

Defining voltage vectors $\mathbf{u}^{\mathrm{A}}$, $\mathbf{u}^{\mathrm{B}}$ and current vectors $\mathbf{i}^{\mathrm{A}}$, $\mathbf{i}^{\mathrm{B}}$, as well as resistance matrices $\mathbf{R}^{\mathrm{A}}$, $\mathbf{R}^{\mathrm{B}}$ for channels A and B, respectively, in the form

$$\mathbf{u}^{\mathrm{A}} = \left[u_1^{\mathrm{A}},u_2^{\mathrm{A}},u_3^{\mathrm{A}}\right]^{\mathrm{T}}, \quad \mathbf{u}^{\mathrm{B}} = \left[u_1^{\mathrm{B}},u_2^{\mathrm{B}},u_3^{\mathrm{B}}\right]^{\mathrm{T}}, \quad \mathbf{i}^{\mathrm{A}} = \left[i_1^{\mathrm{A}},i_2^{\mathrm{A}},i_3^{\mathrm{A}}\right]^{\mathrm{T}}, \quad \mathbf{i}^{\mathrm{B}} = \left[i_1^{\mathrm{B}},i_2^{\mathrm{B}},i_3^{\mathrm{B}}\right]^{\mathrm{T}}, \tag{5}$$

$$\mathbf{R}^{\mathrm{A}} = \mathrm{diag}(R_1^{\mathrm{A}},R_2^{\mathrm{A}},R_3^{\mathrm{A}}), \quad \mathbf{R}^{\mathrm{B}} = \mathrm{diag}(R_1^{\mathrm{B}},R_2^{\mathrm{B}},R_3^{\mathrm{B}}) \tag{6}$$

and making use of definitions (1) and (2), the current-voltage equation and the formula for the electromagnetic torque T_{e} within the framework of the circuit model of DCSRM can be written in the form [6, 9]

$$\begin{bmatrix}\mathbf{u}^{\mathrm{A}}\\ \mathbf{u}^{\mathrm{B}}\end{bmatrix}=\begin{bmatrix}\mathbf{R}^{\mathrm{A}} & \mathbf{0}\\ \mathbf{0} & \mathbf{R}^{\mathrm{B}}\end{bmatrix}\begin{bmatrix}\mathbf{i}^{\mathrm{A}}\\ \mathbf{i}^{\mathrm{B}}\end{bmatrix}+\frac{d}{dt}\left\{\begin{bmatrix}\boldsymbol{\psi}^{\mathrm{A}}(\theta,\mathbf{i}^{\mathrm{A}},\mathbf{i}^{\mathrm{B}})\\ \boldsymbol{\psi}^{\mathrm{B}}(\theta,\mathbf{i}^{\mathrm{A}},\mathbf{i}^{\mathrm{B}})\end{bmatrix}\right\}, \tag{7}$$

$$T_{\mathrm{e}}(\theta,\mathbf{i}^{\mathrm{A}},\mathbf{i}^{\mathrm{B}})=\frac{\partial W_c^*(\theta,\mathbf{i}^{\mathrm{A}},\mathbf{i}^{\mathrm{B}})}{\partial\theta}, \tag{8}$$

where $W_{\mathrm{c}}^*(\theta, \mathbf{i}^{\mathrm{A}}, \mathbf{i}^{\mathrm{B}})$ is the total magnetic field co-energy in the air gap. Equation (8), which is an expression for the electromagnetic torque T_{e} in a three phase DCSRM, under assumptions (3) and (4) can be written in the form [6, 9]

$$\begin{aligned}T_e(\theta,\mathbf{i}^{\mathrm{A}},\mathbf{i}^{\mathrm{B}})=&\sum_{k=1}^{3}\frac{\partial}{\partial\theta}\int_0^{i_k^{\mathrm{A}}}\psi_{kk}^{\mathrm{AA}}(\theta,\bar{i}_k^{\mathrm{A}})\,d\bar{i}_k^{\mathrm{A}}+\sum_{i=2}^{3}\sum_{j=1}^{i-1}\frac{\partial}{\partial\theta}\int_0^{i_i^{\mathrm{A}}}\psi_{ij}^{\mathrm{AA}}(\theta,i_j^{\mathrm{A}})\,d\bar{i}_i^{\mathrm{A}}+\\&+\sum_{k=1}^{3}\frac{\partial}{\partial\theta}\int_0^{i_k^{\mathrm{B}}}\psi_{kk}^{\mathrm{BB}}(\theta,\bar{i}_k^{\mathrm{B}})\,d\bar{i}_k^{\mathrm{B}}+\sum_{i=2}^{3}\sum_{j=1}^{i-1}\frac{\partial}{\partial\theta}\int_0^{i_i^{\mathrm{B}}}\psi_{kk}^{\mathrm{BB}}(\theta,i_j^{\mathrm{B}})\,d\bar{i}_i^{\mathrm{B}}+\\&+\sum_{i=1}^{3}\sum_{j=1}^{3}\frac{\partial}{\partial\theta}\int_0^{i_i^{\mathrm{B}}}\psi_{ij}^{\mathrm{BA}}(\theta,i_j^{\mathrm{A}})\,d\bar{i}_i^{\mathrm{B}}\end{aligned} \tag{9}$$

or, in short,

$$\begin{aligned}T_e(\theta,i_1^{\mathrm{A}},i_2^{\mathrm{A}},i_3^{\mathrm{A}},i_1^{\mathrm{B}},i_2^{\mathrm{B}},i_3^{\mathrm{B}})=&T_{\mathrm{phase}}^{\mathrm{A}}(\theta,i_1^{\mathrm{A}},i_2^{\mathrm{A}},i_3^{\mathrm{A}})+T_{\mathrm{mutual}}^{\mathrm{A}}(\theta,i_1^{\mathrm{A}},i_2^{\mathrm{A}},i_3^{\mathrm{A}})+\\&+T_{\mathrm{phase}}^{\mathrm{B}}(\theta,i_1^{\mathrm{B}},i_2^{\mathrm{B}},i_3^{\mathrm{B}})+T_{\mathrm{mutual}}^{\mathrm{B}}(\theta,i_1^{\mathrm{B}},i_2^{\mathrm{B}},i_3^{\mathrm{B}})+\\&+T_{\mathrm{mutual}}^{\mathrm{BA}}(\theta,i_1^{\mathrm{A}},i_2^{\mathrm{A}},i_3^{\mathrm{A}},i_1^{\mathrm{B}},i_2^{\mathrm{B}},i_3^{\mathrm{B}}).\end{aligned} \tag{10}$$

Individual components of the r.h.s. of Equation (10) representing formula for the resultant torque T_{e} correspond to torque components originating from phase currents ($T_{\mathrm{phase}}^{\mathrm{A}}$, $T_{\mathrm{phase}}^{\mathrm{B}}$) and mutual linkages ($T_{\mathrm{mutual}}^{\mathrm{A}}$, $T_{\mathrm{mutual}}^{\mathrm{B}}$) within channels A and B and the torque related with flux linkages between channels $T_{\mathrm{mutual}}^{\mathrm{BA}}$. In the case of single-channel operation mode, the expression for the torque can be reduced to the first two components of the r.h.s. of Equation (10).

For the purpose of development of a DCSRM simulation model, flux vectors $\boldsymbol{\psi}^{\mathrm{AA}}$ and $\boldsymbol{\psi}^{\mathrm{BB}}$ in Equations (3) and (4) can be separated according to the definition:

$$\boldsymbol{\psi}^{\mathrm{AA}}(\theta,\mathbf{i}^{\mathrm{A}})=\boldsymbol{\psi}_{\mathrm{phase}}^{\mathrm{AA}}(\theta,\mathbf{i}^{\mathrm{A}})+\boldsymbol{\psi}_{\mathrm{mutual}}^{\mathrm{AA}}(\theta,\mathbf{i}^{\mathrm{A}}), \tag{11}$$

$$\boldsymbol{\psi}^{\mathrm{BB}}(\theta,\mathbf{i}^{\mathrm{B}})=\boldsymbol{\psi}_{\mathrm{phase}}^{\mathrm{BB}}(\theta,\mathbf{i}^{\mathrm{B}})+\boldsymbol{\psi}_{\mathrm{mutual}}^{\mathrm{BB}}(\theta,\mathbf{i}^{\mathrm{B}}). \tag{12}$$

where the individual components represent, respectively, the phase fluxes (subscript ‘phase’) and the mutual linkage fluxes between the phases (subscript ‘mutual’) with respect to the given channels A and B according to the relationships

$$\boldsymbol{\psi}^{\mathrm{AA}}_{\mathrm{phase}}(\theta,\mathbf{i}^{\mathrm{A}})=\begin{bmatrix}\psi^{\mathrm{AA}}_{11}(\theta,i^{\mathrm{A}}_1)\\ \psi^{\mathrm{AA}}_{22}(\theta,i^{\mathrm{A}}_2)\\ \psi^{\mathrm{AA}}_{33}(\theta,i^{\mathrm{A}}_3)\end{bmatrix},\quad \boldsymbol{\psi}^{\mathrm{AA}}_{\mathrm{mutual}}(\theta,\mathbf{i}^{A})=\begin{bmatrix}\psi^{\mathrm{AA}}_{12}(\theta,i^{\mathrm{A}}_2)+\psi^{\mathrm{AA}}_{13}(\theta,i^{\mathrm{A}}_3)\\ \psi^{\mathrm{AA}}_{21}(\theta,i^{\mathrm{A}}_1)+\psi^{\mathrm{AA}}_{23}(\theta,i^{\mathrm{A}}_3)\\ \psi^{\mathrm{AA}}_{31}(\theta,i^{\mathrm{A}}_1)+\psi^{\mathrm{AB}}_{32}(\theta,i^{\mathrm{A}}_2)\end{bmatrix}, \tag{13}$$

$$\boldsymbol{\psi}^{\mathrm{BB}}_{\mathrm{phase}}(\theta,\mathbf{i}^{\mathrm{B}})=\begin{bmatrix}\psi^{\mathrm{BB}}_{11}(\theta,i^{\mathrm{B}}_1)\\ \psi^{\mathrm{BB}}_{22}(\theta,i^{\mathrm{B}}_2)\\ \psi^{\mathrm{BB}}_{33}(\theta,i^{\mathrm{B}}_3)\end{bmatrix},\quad \boldsymbol{\psi}^{\mathrm{BB}}_{\mathrm{mutual}}(\theta,\mathbf{i}^{\mathrm{B}})=\begin{bmatrix}\psi^{\mathrm{BB}}_{12}(\theta,i^{\mathrm{B}}_2)+\psi^{\mathrm{BB}}_{13}(\theta,i^{\mathrm{B}}_3)\\ \psi^{\mathrm{BB}}_{21}(\theta,i^{\mathrm{B}}_1)+\psi^{\mathrm{BB}}_{23}(\theta,i^{\mathrm{B}}_3)\\ \psi^{\mathrm{BB}}_{31}(\theta,i^{\mathrm{B}}_1)+\psi^{\mathrm{BB}}_{32}(\theta,i^{\mathrm{B}}_2)\end{bmatrix}. \tag{14}$$

Figure 3 shows a block diagram representing schematically structure of the simulation model based on voltage-current equations (7) in a dual-channel DCSRM with mutual linkages both between phases of individual channels (A or B) and between phases of different channels taken into account.

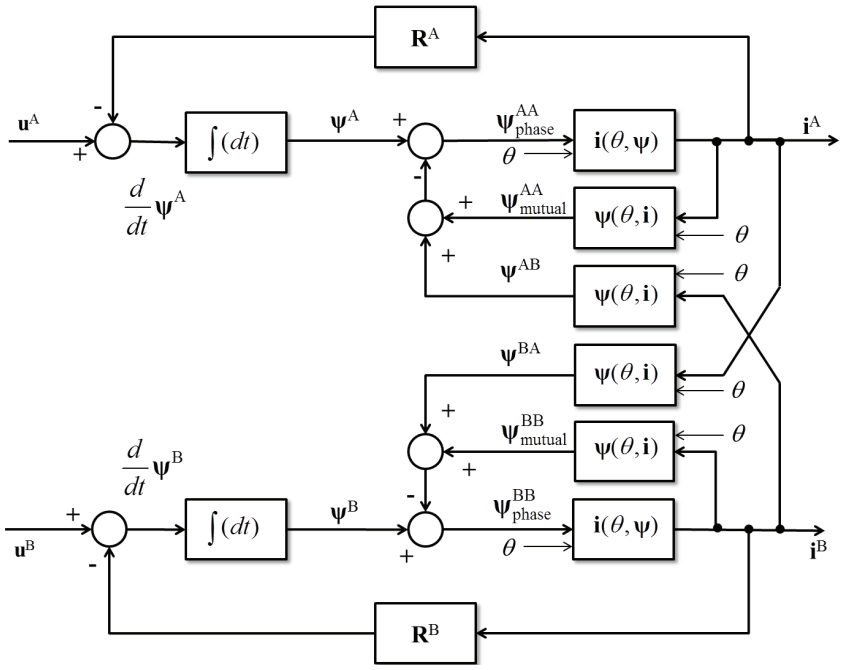

Fig. 3. A schematic diagram of the simulation model based on voltage-current equations of a DCSRM

Functional dependencies of the fluxes on the rotor position and current in given phase represented by Equations (3) and (4) as well as in the formula for the electromagnetic torque given by Equation (9) are most often calculated with the use of the field approach. They are described with the use of various techniques, e.g. analytically by means of series of the variable θ with coefficients depending on the current, or numerically in the form of look-up tables or artificial neural networks (ANN).

Based on Equations (7) and (9), a simulation model in Matlab/Simulink system [6] has been developed. Functional dependencies of individual fluxes on the rotor position and currents in relevant phases occurring in Equation (7) and in Equation (9) representing a formula for the torque were determined by means of 2D field calculations. They are described in a tabular form with the use of 2-D Look-Up Table blocks from Simulink's library. Simulation studies carried out for a model DCSRM with 12/8 configuration involved calculations of the so-called static characteristics and, as far as time-dependency is concerned, analyses of voltage, current, and the torque waveforms. Operation of the motor was examined in both single- and dual-channel operation mode for constant rotor speed.

3. Analysis of DCSRM static characteristics

3.1. Magnetic field distribution in a three-phase DCSRM

Simulation studies on the magnetic field distribution patterns by means of the Finite Element Method were carried out in 2D for a 12/8 three-phase dual channel DCSRM [7]. Magnetic field distribution analysis was carried out for different rotor positions starting from the so-called unaligned position, i.e. the rotor position angle assumed conventionally as $\theta = 0$, up to the so-called aligned position, corresponding to angle $\theta = \pi/8$. Calculations were carried out for the motor operating in the dual-channel mode, for both different and equal values of currents in channels A and B from the range (0 A, 10 A) under single-channel operation mode.

Dual-channel operation mode

Figure 4 shows example distribution patterns of magnetic flux lines for the dual-channel operation mode under assumption that only the first phases of both channels, A and B, with phase currents being fixed and equal to each other, $i_1^A = i_1^B = 10$ A for three rotor position angles, i.e. $\theta = 0$, $\theta = \pi/18$, and $\theta = \pi/8$, producing flux distribution patterns shown on Figures 4(a), 4(b), and 4(c), respectively.

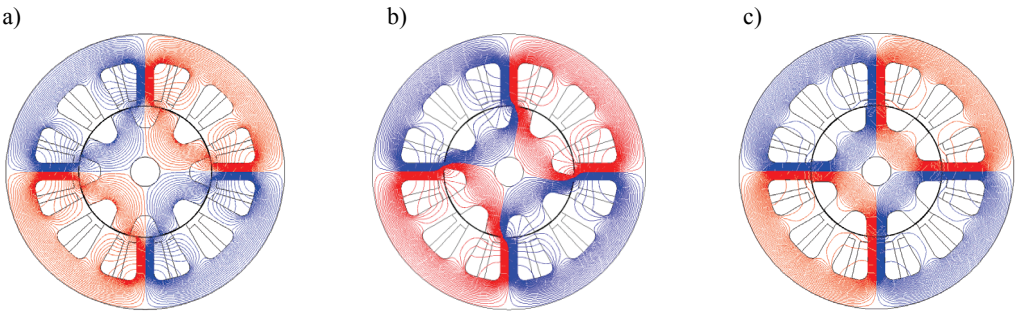

Fig. 4. Magnetic field distributions patterns for $i_1^A = i_1^B = 10$ A and: a) $\theta = 0$; b) $\theta = \pi/18$; c) $\theta = \pi/8$

Magnetic fluxes in the examined DCSRM follow the so-called short or long flux paths, which has an essential effect on resultant properties of the machine, and on the produced electromagnetic moment in particular.

Single-channel operation mode

Examples of the flux distribution patterns under single-channel operation mode for rotor position angles $\theta = 0$, $\theta = \pi/18$, and $\theta = \pi/8$ under the assumption that only the first phase of channel A is supplied with current $i_1^A = 10$ A are presented in Figure 5.

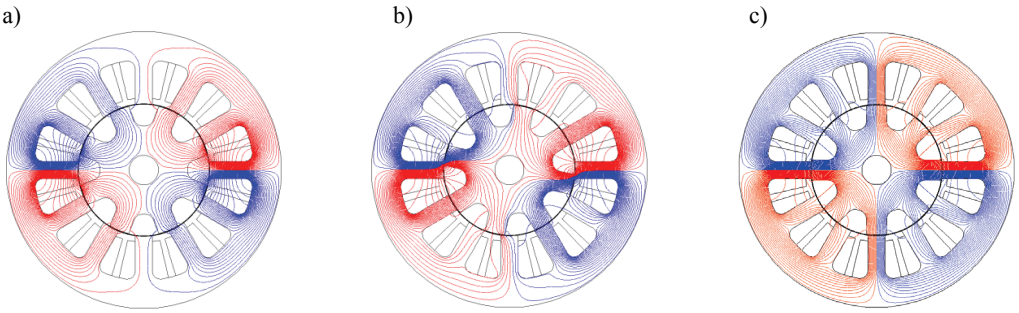

Fig. 5. Magnetic field distributions patterns for $i_1^A = 10$ A, $i_1^B = 0$ A, and: a) $\theta = 0$; b) $\theta = \pi/18$; c) $\theta = \pi/8$

From analysis of the magnetic field distribution patterns, one may draw a conclusion that with DCSRM operation in the dual-channel mode and under the assumption of equality of currents in corresponding phases of channels A and B, the resultant fluxes in the conducting poles of a given channel's phases depend only on currents of these phases as the fluxes induced by currents of the remaining phases virtually cancel each other out.

Based on field theory calculations for individual phases of both channels A and B, the so-called static characteristics of the motor were determined, i.e. phase self- and mutual fluxes and the resultant electromagnetic torque as functions of the current and the rotor position.

3.2. Static characteristics of the three-phase DCSRM

Based on field theory calculations for individual phases of both channels A and B, phase self- and mutual fluxes and the torque were determined as functions of the current and the rotor position angle.

Dual-channel operation mode

Figures 6 and 7 present example calculation results for flux characteristics, and Figure 8 shows a plot of motor torque T_e for dual-channel operation mode under the assumption that currents in both phases of channels A and B have the same intensity ($i_1^A = i_1^B$).

Single-channel operation mode

In Figures 9 and 10, calculation results for selected flux characteristics are presented, while Figure 11 shows a plot of motor torque T_e, all under single-channel operation mode.

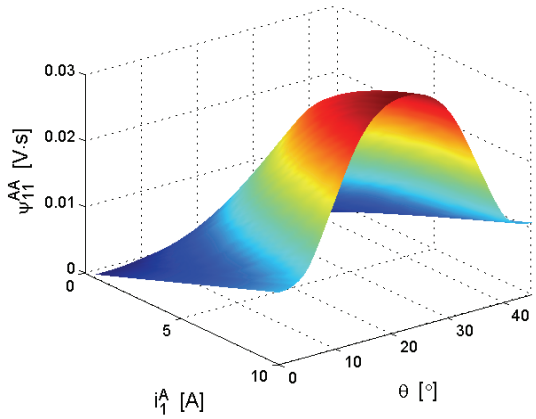

Fig. 6. The current-angle characteristics of flux ψ_{11}^{AA} under dual-channel operation mode

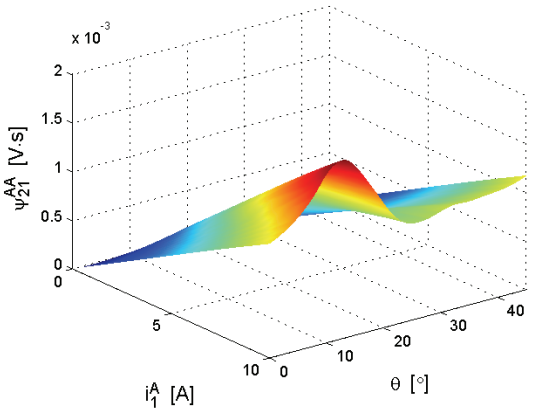

Fig. 7. The current-angle characteristics of flux ψ_{21}^{AA} under dual-channel operation mode

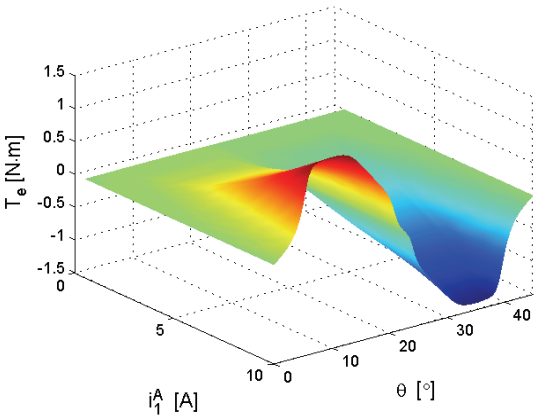

Fig. 8. Torque T_e as a function of current i_1^A and angle θ under dual-channel operation mode

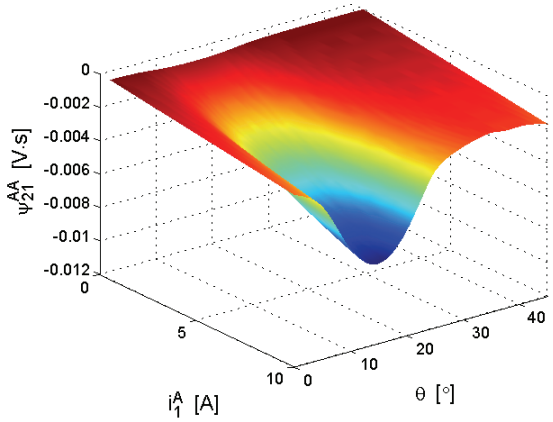

Fig. 9. The current-angle characteristics of flux ψ_{21}^{AA} under single-channel operation mode

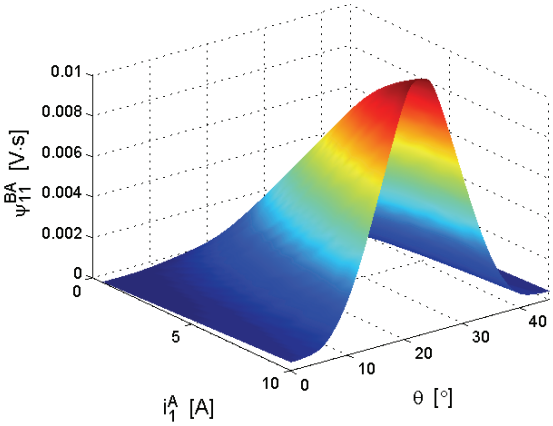

Fig. 10. The current-angle characteristics of flux ψ_{11}^{BA} under single-channel operation mode

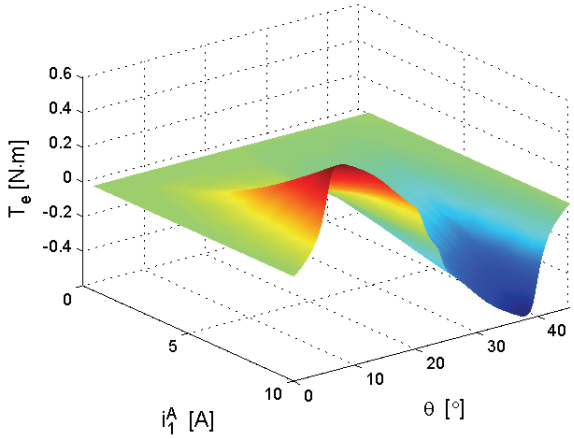

Fig. 11. Torque T_e as a function of current i_1^A and angle θ under single-channel operation mode

It can be seen from comparing Figures 8 and 11 that the resultant motor static torque in dual-channel operation mode for the same phase current values in both channels is more than twice as large as this in the single-channel operation mode.

4. Analysis of DCSRM voltage, current, and torque waveforms

Simulations of voltage, current, and torque waveforms were carried out for the machine supplies in dual-channel and single-channel mode. By way of an example, under dual-channel operation mode, Figure 12 shows simulations results in the form of voltages and currents in individual phases of channel A as functions of the rotor position θ, whereas Figure 13 is a plot of the supply current as a function of the same variable. The resultant motor electromagnetic torque as a function of the rotor position for the dual-channel operation is presented in Figure 14.

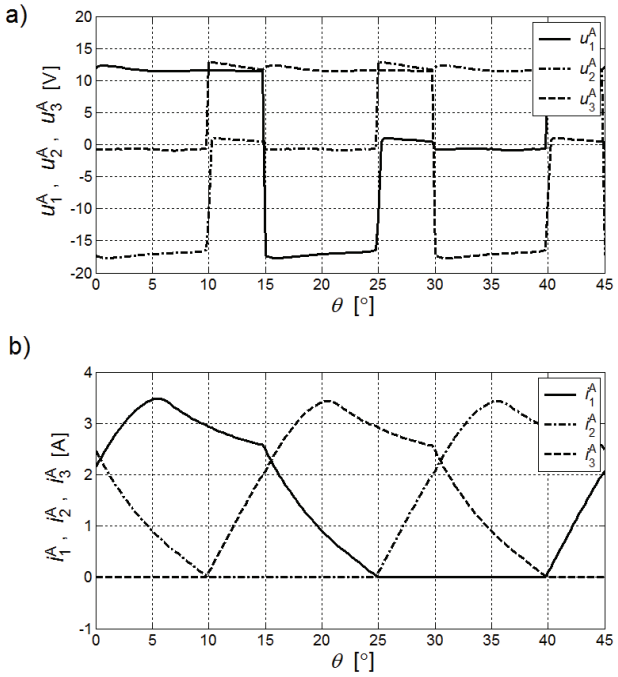

Fig. 12. Phase voltages a) and currents b) of channel A as functions of the rotor position under dual-channel operation

For the single-channel operation mode, channel A phase voltages and currents as functions of the rotor position θ are shown in Figure 15. Similarly, Figure 16 presents waveforms of voltages induced in three phases of channel B for the single-channel operation mode, i.e. with channel A being supplied. Further, Figure 17 shows a plot of the supply current as a function

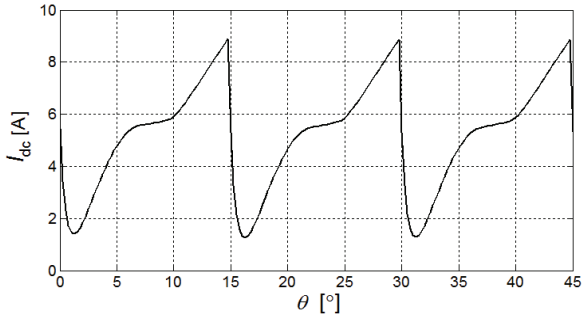

Fig. 13. The supply current as a function of the rotor position under dual-channel operation

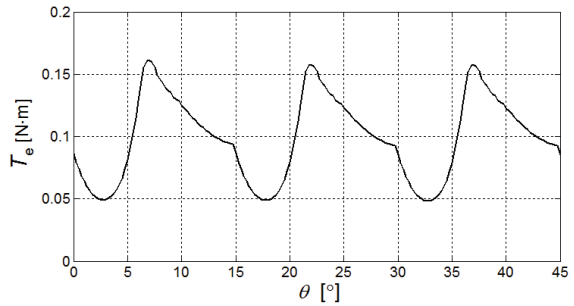

Fig. 14. The torque as a function of the rotor position under dual-channel operation

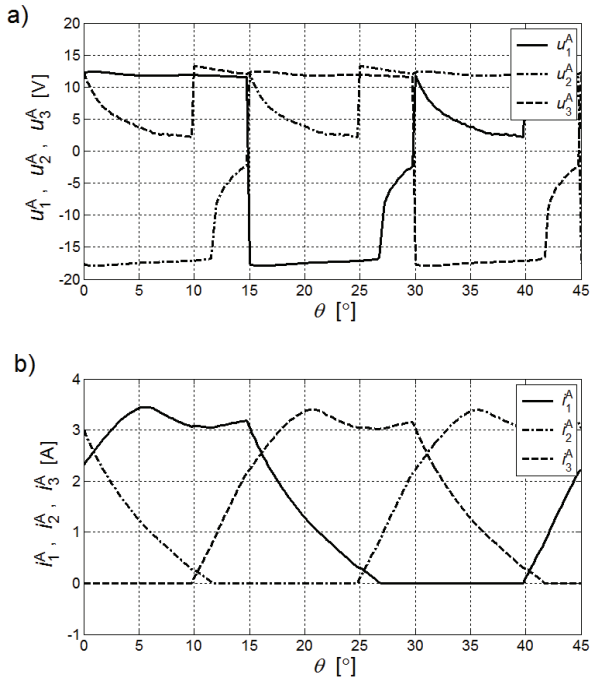

Fig. 15. Voltages a) and currents b) as functions of the rotor position under single-channel operation mode

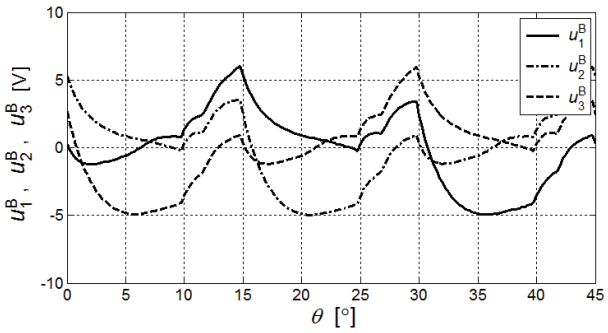

Fig. 16. Voltages induced in channel B phases as functions of the rotor position angle under single-channel operation mode

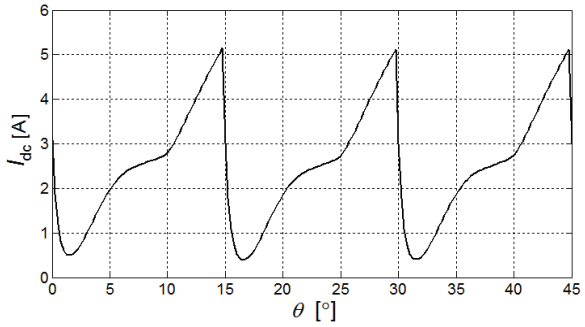

Fig. 17. The supply current as a function of the rotor position under single-channel operation mode

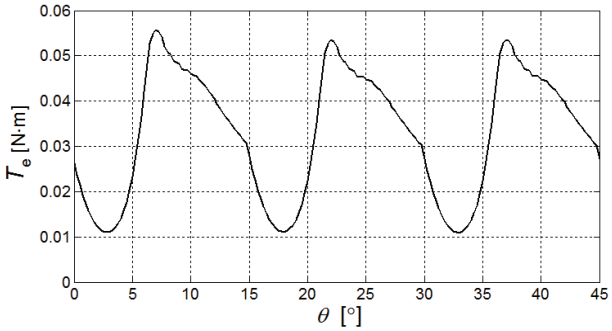

Fig. 18. Channel B torque as a function of the rotor position under single-channel operation mode

of rotor angle θ, while Figure 18 presents the torque produced by the motor's channel A as a function of the same parameter under single-channel operation mode.

The average torque value T_{eav} of Figure 18 is almost three times lower than that obtained in the case of the dual-channel operation mode (Fig. 14).

5. Results of laboratory tests with a DCSRM model

Laboratory tests were carried out with a model of DCSRM designed by the present authors. An overview of the machine is shown in Figure 19a, whereas a view of the stator and the rotor with the bearing disk is presented in Figure 19b.

a) b)

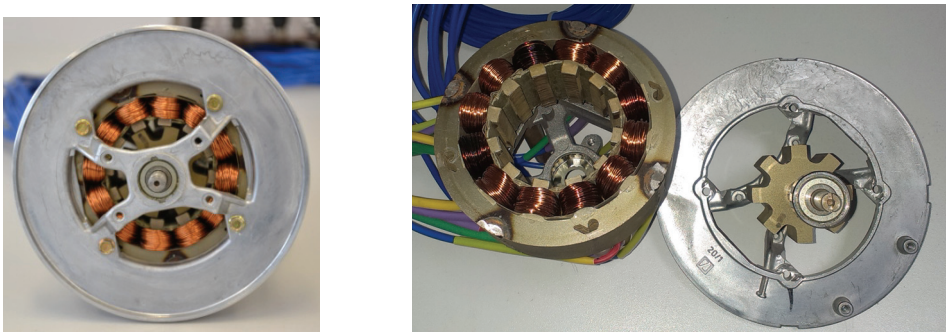

Fig. 19. The DCSRM model: a) stator; b) rotor

The torque-current-angle characteristics measured for different current values are shown in Figures 20 and 21 under dual- and single-channel operation mode, respectively. Figure 22 presents plots of the motor torque average value T_{eav} as a function of current I under single-channel and dual-channel operation mode.

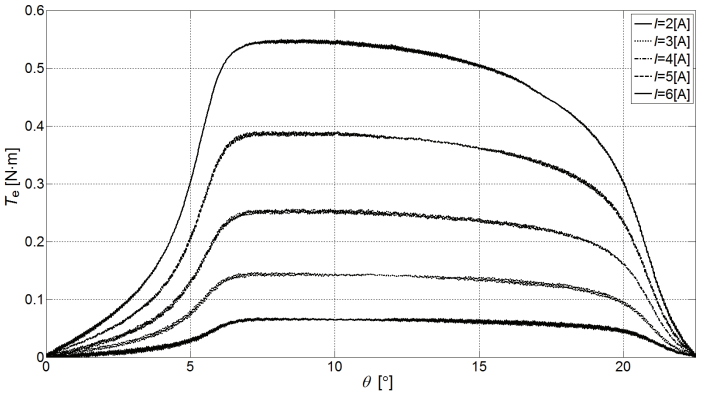

Fig. 20. Static torque-angle characteristics for different current values under dual-channel operation mode

It follows from the static characteristics presented in Figures 20 and 21 that the torque produced in the dual-channel operation mode is more than twice as large as the one observed under the single-channel operation mode which is a feature consistent with the results of the simulation calculations.

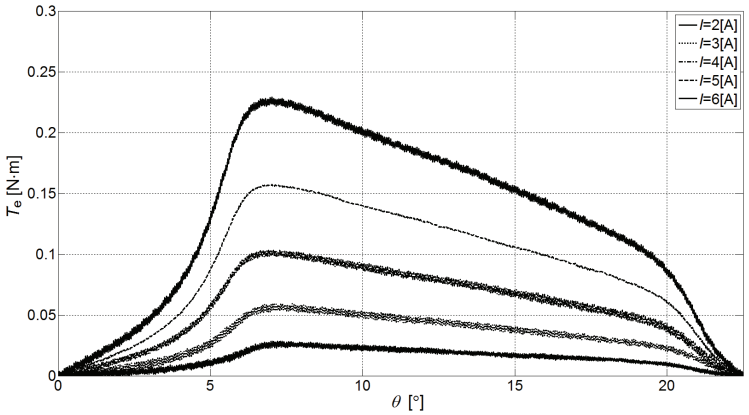

Fig. 21. Static torque-angle characteristics for different current values under single-channel operation mode

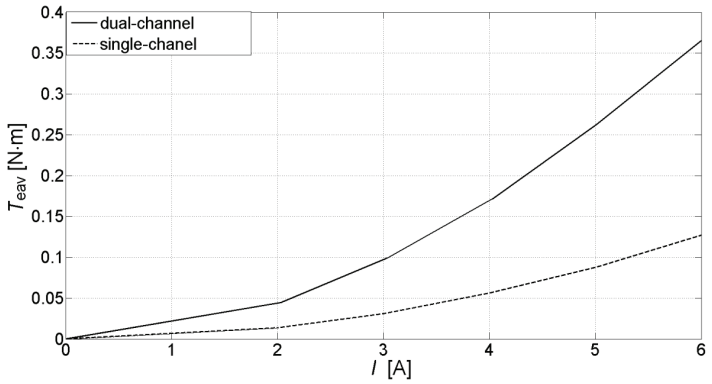

Fig. 22. Torque average value as a function of current under dual-channel and single-channel operation mode

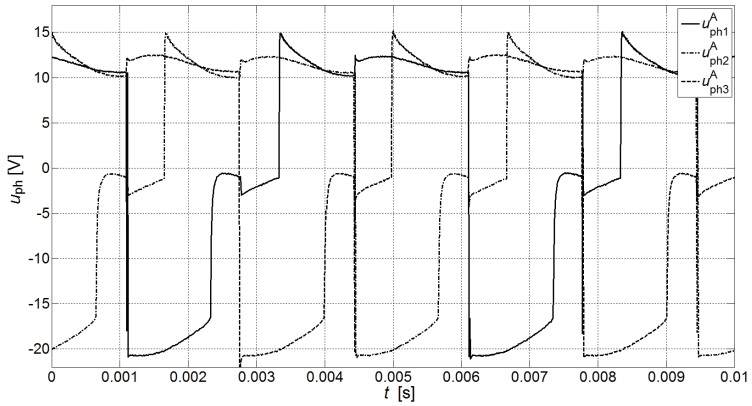

Fig. 23. Channel A phase voltage waveforms under dual-channel operation mode

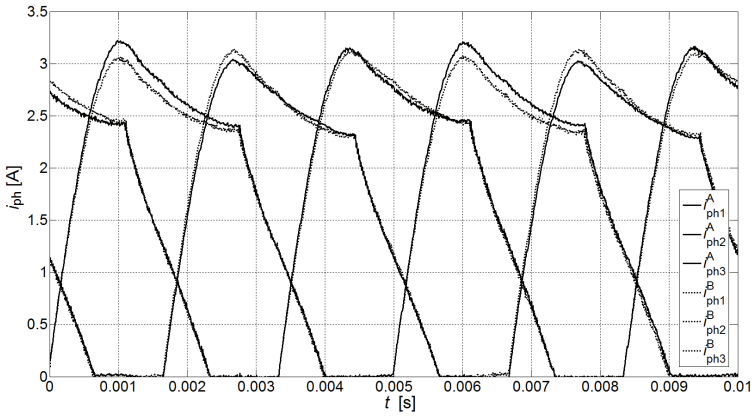

Fig. 24. Channel A and B phase current waveforms under dual-channel operation mode

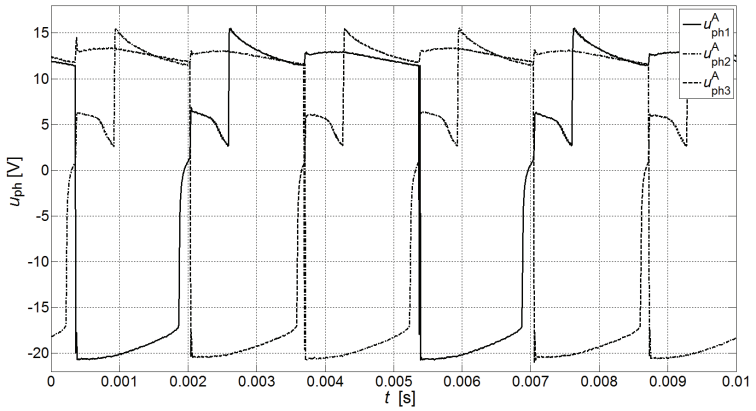

Fig. 25. Channel A phase voltage waveforms under single-channel operation mode

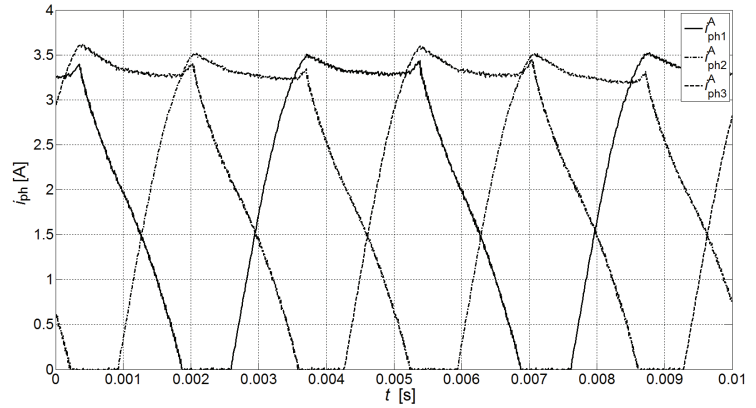

Fig. 26. Channel A phase current waveforms under single-channel operation mode

Figures 23 and 24 show plots of waveforms measured on the model and representing voltages and currents, respectively, of the three motor phases under dual-channel operation mode.

Measured waveforms of the three phase voltages and the three phase currents are shown in Figures 25 and 26, respectively, for channel A under single-channel operation mode, while Figure 27 is a plot of waveforms representing voltages induced on open terminals of individual phases of channel B.

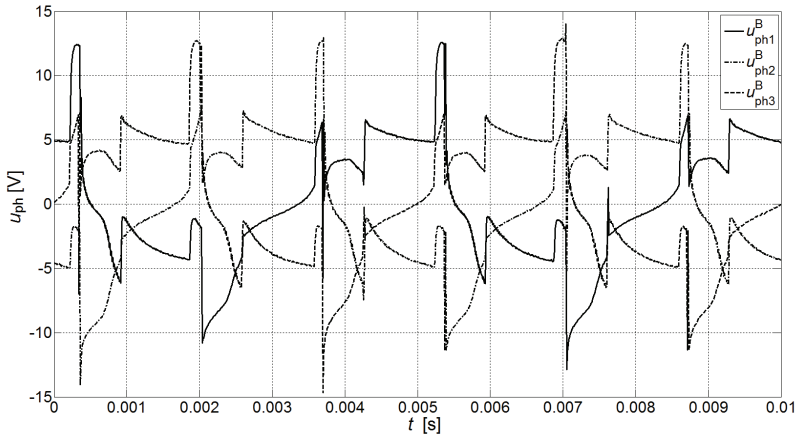

Fig. 27. Waveforms of voltages induced in channel B with channel A operating under single-channel mode

6. Conclusions

On the grounds of the research results presented above, the following conclusions can be drawn:

- The mathematical model of dual-channel switched reluctance motor proposed in this paper takes into account all linkages occurring between individual phases of both channels and allows to develop a simulation model capable to reproduce operation of DCSRM under both dual-channel and single-channel mode.
- In dual-channel operation mode, the resultant motor torque is about 2.5 times larger than this obtained in the single-channel operation mode and must not be calculated by means of simple adding the two torques produced by phase currents of both channels, but the torque relating to fluxes corresponding to linkages between channels must also be taken into account.
- Both static characteristics and time-dependent waveforms measured on a laboratory model of DCSRM confirm fully the usefulness of the machine for operation in both dual-channel and single-channel mode.

Further research, both simulations and laboratory tests, are required to analyse DCSRM performance in the case of an asymmetry of supplying and/or controlling both channels, also in electric failure conditions.

References

[1] Radun A.V., Ferreira C.A., Richter E., *Two-channel Switched Reluctance Starter/Generator Results.* IEEE Transactions on Industry Applications 34(5): 1026-1034 (1998).

[2] Ding W., Liang D., *Calculation of Flux Linkages of a 12/8 Dual-Channel SRM Including Mutual Coupling and Saturation: From Magnetic Circuit Model to FEM Analysis.* Industry Applications Society Annual Meeting, IAS '08. IEEE, 2008 , pp. 1-8 (2008).

[3] Ding W., Liang D., *Comparison of transient and steady-state performances analysis for a dual-channel switched reluctance machine operation under different modes*. Electric Power Applications, IET 4(8): 603-617 (2010).

[4] Ding W, Liang D, Sui H., *Dynamic Modeling and Performance Prediction for Dual-Channel Switched Reluctance Machine Considering Mutual Coupling.* IEEE Transactions on Magnetics 46(9): 3652-3663 (2010).

[5] Ding W., *Comparative Study on Dual-Channel Switched Reluctance Generator Performances Under Single- and Dual-Channel Operation Modes.* IEEE Transactions on Energy Conversion 27(3): 680-688 (2012).

[6] Prokop J., *Mathematical models of multiphase dual-channel switched reluctance machines.* Przegląd Elektrotechniczny 2: 149-156 (2012) (in Polish).

[7] Bogusz P., Korkosz M., Prokop J., *Static characteristics analysis of dual-channel switched reluctance machine.* Przegląd Elektrotechniczny 7a: 206-213 (2012) (in Polish).

[8] Bogusz P., Korkosz M., Prokop J., *Mutual coupling analysis influence on dual-channel switched reluctance motor properties*. Przegląd Elektrotechniczny 8: 309-316 (2012) (in Polish).

[9] Prokop J., *Mathematical Modeling of Switched Electric Machines*. (book in Polish: *Modelowanie matematyczne maszyn elektrycznych przełączalnych*), Oficyna Wydawnicza Politechniki Rzeszowskiej, Rzeszów (2013) (Poland).

[10] Ding W., Liu L., Lou J., Liu Y., *Comparative Studies on Mutually Coupled Dual-Channel Switched Reluctance Machines With Different Winding Connections.* IEEE Transactions on Magnetics 49(11): 5574-5589 (2013).

[11] MATLAB Documentation, MathWorks (2012).